Microstructural analyses of artificial ageing in 5 commercially and non-commercially available Zirconia dental implants

Mona Monzavi, Fei Zhang, Thierry Douillard, Laurent Gremillard, Sammy Noumbissi, Hessam Nowzari, Jérome Chevalier

Microstructural analyses of artificial ageing in 5 commercially and non-commercially available Zirconia dental implants

Published in the Journal of the European Ceramic Society 40 [10], 2020, pp. 3642-3655
https://doi.org/10.1016/j.jeurceramsoc.2020.03.050

Mona Monzavi[ab], Fei Zhang[b], Thierry Douillard[b], Laurent Gremillard[b], Sammy Noumbissi[c], Hessam Nowzari[a], Jerome Chevalier[b]

[a] Private Practice, 120 S Spalding Drive, Beverly Hills, CA, 90212, USA
[b] Université de Lyon, INSA-Lyon, UMR CNRS 5510 MATEIS, 7 Avenue Jean Capelle, 69621 Villeurbanne Cedex, France
[c] International Academy of Ceramic Implantology Zirconia Implant Research Group-ZIRG, 801 Wayne Avenue, Suite G200 Silver Spring, MD 20910 USA

Abstract

Objectives

The present *in vitro* study evaluated the effect of LTD (Low Temperature Degradation) on microstructural properties, phase transformation and micro-crack formation of 5 commercially and non-commercially available Zirconia dental implant systems.

Methods

Accelerated ageing at 134 °C and 2 bar pressure for 30 h was completed. Focused Ion Beam-Scanning Electron Microscopy (FIB/SEM), X-ray diffraction (XRD) and cathodoluminescence quantified phase transformation and micro-crack formation.

Results

Transformation of the tetragonal grains towards the monoclinic symmetry was observed in all systems. The highest depth was measured in non-commercial TAV dental with the largest grain size (8.7 μm). A micro-cracked layer was associated with the transformation zone. The ageing-related micro-crack formation was parallel to the surface for all groups and was deepest for the non-commercial TAV dental with the largest grain size (7.4 μm).

Conclusion

LTD following *in vitro* ageing using an autoclave was minimal for all implant systems investigated.

Keywords

Zirconia dental implant ; Artificial ageing ; Low temperature degradation ; FIB-SEM ; X-ray diffraction (XRD)

1. Introduction

The claims over superior esthetic outcome, lesser plaque accumulation, and no metal sensitization have led to increased popularity of Zirconia dental implants as an alternative to titanium [1,2,3,4]. Zirconia (ZrO_2) crystal structure is temperature dependent and polymorphic [5]. At room temperature, it exists in its monoclinic phase and transforms to tetragonal above 1170 °C and cubic at 2370 °C [5]. Stabilizing the tetragonal phase at room temperature allows for stress induced transformation toughening mechanism, which resists crack propagation [5,6]. The metastable tetragonal ceramics demonstrate remarkable toughness when the transformation to monoclinic phase is triggered by a propagating crack [7]. This finding gave rise to the development of high toughness ceramics namely yttria-stabilized tetragonal zirconia polycrystal (Y-TZP). On the other hand, it was later discovered that due to its metastability, in presence of water molecules, Y-TZP may undergo a slow tetragonal-monoclinic phase transformation (t-m transformation) at low temperatures followed by surface roughening, intergranular micro-cracking, grain pull out and loss of strength, referred to as low temperature degradation "LTD" or "ageing" [8].

In 2001, the failure of several hundreds of hip prostheses was reported, which led to the termination of Y-TZP in orthopedics [9,10]. Nevertheless, following significant improvements, Y-TZP gained popularity in dental applications, including dental implants and restorative prostheses [11,12,13] due to its superior aesthetic, biocompatibility, mechanical properties, and low plaque affinity. LTD in dental zirconia is a new topic supported by only few studies [14,15]. Recent *in vitro* studies showed that Y-TZP dental ceramics were susceptible to LTD, which resulted in increased surface roughness [16,17], and micro-cracking in the bulk [18] or both bulk and porous coatings [19]. The practical consequences of such extensive micro-cracking in terms of dental implants may be exfoliation of the surface porous layer and delamination from the bulk, which may further result in loss of integration [19]. In terms of the effects of LTD on the strength of zirconia, the results are quite variable. A review article on orthopedic implants revealed that strength of zirconia could decrease or increase by aging [3]. Other studies revealed a reduction in Young's modulus and hardness [16,20] of aged surfaces and reduction of flexural strength [21]. Further recent studies demonstrated that a considerable degree of t-m transformation did not lead to a decrease in strength [22] or even led to a significant increase in strength [18,19,23]. Regardless of available contradictory results on strength, its verified influence on structural integrity in terms of micro-cracking and increased surface roughness may influence its interaction with surrounding bone and soft tissue. Therefore, it is important to accurately characterize the effect of LTD on surface and bulk of dental implants. Features of surface topography as a result of roughening procedures may facilitate water penetration and ageing [18]. A recent investigation suggested that resistance to ageing may be more related to structural details and composition than the features of surface topography as a result of surface roughening procedures [24].

Furthermore, although zirconia dental implants are processed in accordance with the ISO 13356, due to the manufacturing variability, dental implants from different manufacturers may behave differently. According to our knowledge, there is no such comparative and systematic study performed by the same group of researchers on commercially available zirconia implants available so far. The present study evaluated the effect of LTD on microstructural properties of 5 commercially available zirconia dental implants *in vitro*. There is also a common notion that grain size plays a pivotal role on LTD kinetics [14]. The present study also aims at evaluating the effect of changes in the grain size from the nominal one, thought remaining within the ISO recommendation on LTD. Therefore, two non-commercially available modalities of one type

of implants were prototypes, for which the sintering temperature was intentionally increased with the rationale to investigate the effect of grain size on ageing kinetics.

The null hypotheses of this work are thus that:

- Increase in grain size due to subtle changes in the sintering process is not correlated to increase in depth of transformation and microcracking.

- There are no significant micro-structural differences between groups following ageing, despite their differences in surface preparation and processing.

2. Materials and methods

2.1. Implant description

Five commercially and two non-commercially available zirconia dental implant systems, processed under ISO 13356, were investigated. With the exception of Zeramex (Zeramex® Dental point, Zurich) group, all other implants were made from 3 mol % yttria- stabilized zirconia powder. Two implants were used within each group (one prior to ageing and one following ageing). Table 1 summarizes the implants and their manufacturing processing. The Z-systems® (Oensingen, Switzerland) implants were fabricated using hot isostatic pressing, sandblasting and laser modification. The fabrication process for Straumann® (Basel, Switzerland) consisted of hot isostatic pressing, sand blasting and etching with hydrofluoric acid. The Zibone® (Taiwan) fabrication process consisted of injection molding, sintering, and sandblasting. The TAV Dental® implants (Shlomi, Israel) were manufactured using ceramic injection-molding and sintering. Three implant types were provided by TAV Dental manufacturer. Group 1 was commercially available with grain size of 0.4 μm. Group 2 (grain size: 0.49 μm) and group 3 (grain size: 0.6 μm) were prototypes, for which the sintering temperature was intentionally increased with the rationale to investigate the effect of grain size on ageing kinetics. These materials were developed with the hypothesis that increase in grain size will lead to higher rate of grain transformation following low temperature degradation which will then lead to increased microcrack formation. Note that even the implants with the largest grain size would meet the ISO 13356 recommendations. The Zeramex implants (Zeramex® Dental point, Zurich) were full ceramic made of alumina-zirconia 3Y-TZP composite.

2.2. Accelerated ageing test

Implants were unpacked and cleaned by ethanol prior to ageing. The established accelerated ageing process was conducted at 134 °C and 2 bar pressure in water steam for 30 h. Prior to increasing the temperature, atmospheric air was evacuated to ensure 100 % humidity. Ageing in autoclave has often been used as a tool to accelerate ageing and to assess the resistance to LTD of a given 3Y-TZP based material. It is used in ISO recommendations, which requires no more than 25 vol.% of monoclinic phase measured by X-Ray diffraction after 5 h at 134 °C, 2 bars. From time-temperature equivalence and the knowledge of the activation energy of LTD at relatively low temperature, it has been calculated and often considered that one hour in autoclave at 134 °C would be roughly equivalent to 1–4 years at 37 °C [10]. The conditions explored in this study would represent therefore long duration at 37 °C. They will be debated in the discussion section.

Table 1: Implants investigated in this work and their manufacturing processing.

	Initial powder, Process history[#]	Grain size of zirconia (SD)[*]	Sand blasting	Etching	Laser treatment	Additional treatment	Sterilization
Z-Systems®, Z5c Zirkolith®, Oensingen, Switzerland	TZP-A Isostatic compaction, sintering, HIP, grinding	0.42 (0.03) µm	Al_2O_3[*]	No	SLM patented	Sintering	Plasma sterilization
Straumann® Pure Ceramic Implant, Basel, Switzerland	TZP-A, spray drying, Cylinder pressing, sintering, HIP, machining	0.22 (0.04) µm	ZrO_2 Large grit	Hydrofluoric acid	No	No information	No Information
Zibone®, Coho Biomedical Technology Co. Ltd, Taiwan	TZP-A, Injection molding, sintering, grinding	0.39 (0.03) µm	ZrO_2	No	No	Annealing	No information
TAV Dental®, Shlomi, Israel	TZP-A, Injection molding, sintering	0.4 (0.02) /0.47 (0.03) /0.65 (0.04) µm	No information	No information	No	No information	No information
Zeramex® Dental point, Zurich, Switzerland	ATZ powder, HIP	0.47 (0.03) µm	ZrO_2[*]	yes	No	No information	No information

TZP-A, A refers to a light amount of alumina addition in the range of 0.2−0.25 wt.% in the starting powder.
* Information was obtained in this study from SEM images shown in Fig. 1.

2.3. X-ray diffraction

The X-ray diffraction (XRD) technique was utilized to measure the monoclinic content at the surface of the implants prior to ageing and after 30 h of ageing, using a Bruker D8 advance diffractometer (Bruker, Karlsruhe, Germany) with the assistance of microfocus laser. The XRD patterns were collected using CuK_α radiation (40 kV and 50 mA), θ-2θ mode (Bragg-Brentano symmetrical configuration, 2θ in the [27°-33°] range), scan speed of 0.2°/min and 0.02° step size. The estimated depth of analysis with such configuration is around 5 µm below the surface [25]. In addition to surface evaluation, XRD was completed on mechanically polished cross sections of the implants (before and after ageing) to determine the core t-m transformation. The implants were sectioned in two halves with a water-cooled diamond wire saw (Model 3242, Well, Switzerland) and flattened with 10 µm diamond discs and sequentially polished with 7, 3, and 1 µm diamond pastes and 0.5 µm colloidal silica on an EcoMet250 (Buehler, LakeBluff, IL, US). The Toraya's Garvie and Nicholson's equations were used to calculate the monoclinic contents on both the surface and polished cross sections. The volume was then determined using the following formula:

$$f = \frac{1.311X_m}{1+0.311X_m} \qquad (1)$$

$$X_m = \frac{I_m^{(\bar{1}11)}+I_m^{(111)}}{I_m^{(\bar{1}11)}+I_m^{(111)}+I_t^{(101)}} \qquad (2)$$

With X_m the integrated intensity ratio, $I_m{}^{(h\,k\,l)}$ the area of the (h k l) peak of the monoclinic phase and $I_t{}^{(h\,k\,l)}$ the area of the (h k l) peak of the tetragonal phase.

Using these equations and experimental conditions, a detection limit for *f* below 1% is expected on polished cross section surfaces (2% on intact implant surfaces), while the absolute precision is also around ±1% (±3% on intact implant surfaces).

2.4. Microstructural characterization

Surface microstructural characteristics of Zirconia implants were examined prior to ageing and after 30 h of ageing using Scanning Electron Microscopy (SEM). Further evaluations of implant subsurface prior to and after ageing, in terms of induced transformation and micro-crack formation were completed on focused ion beam (FIB) cross-sections. These experiments were performed using a FIB/SEM workstation (NVision 40; Carl Zeiss Microscopy GmbH, Oberkochen, Germany) combining a SIINT zeta FIB column (Seiko Instruments Inc. NanoTechnology, Japan) with a Gemini I column. FIB was used to provide cross sections at the top of the threads.

To minimize the curtain effect introduced by the gallium ion beam milling (*i.e.* vertical stripes on the cross- section induced by ion milling) and to protect the sample surface from implantation, an in-situ ion beam induced deposition was performed over the areas of interest with phenanthrene C4H10 as a precursor gas (sputter-resistant layer of about 1 µm).

Subsequently, trenches were milled to a depth that freed up a cross-sectional surface allowing assessing the LTD depth (width of 20 µm and depth between 15 and 20 µm). Settings for 30 kV ion accelerating voltage with decreasing beam currents (27 nA, 13 nA, 1.5 nA and 700 pA) and probe sizes were used to reach a suitable cross-section for SEM imaging and to avoid any ion beam induced monoclinic transformation. The FIB gun was operated around 90 min for each cross-section.

SEM imaging was performed at 1.5KeV simultaneously with Secondary Electron (SE) and Energy filtered Backscattered Electron (BSE).

One cross-section was made for each implant at the top of the threads except for the Zibone implant. For this last implant, two cross-sections were done: one on flattened surface related to sandblasting, the other on a surface spared by sandblasting. BSE signals leads to a strong crystallographic contrast imaging which is useful for identifying signs of twinning associated to tetragonal–monoclinic transformation. The SE imaging allowed to better visualize micro-cracks.

Cathodoluminescence (CL) imaging in SEM (SEM-CL) was performed on mechanically sectioned and polished samples of Z systems®, Straumann® and Zibone® to visualize the spatial distribution of monoclinic phase within tetragonal zirconia. Nickel plating process was implemented to protect the surface from the machining steps. To make the surface electrically conductive, the samples were first coated with a gold layer of 30 nm by sputtering (EM SCD500, Leica Microsystems GmbH, Germany). The pieces were then immersed into a Nickel Sulfate electrolyte (Watts bath) and used as cathode, whereas a nickel anode was dissolved. The cathode current density was set to 2A/dm² during 30 min in order to reach a thickness of nickel of around 30 µm according to the Faraday's Law. After this nickel electroplating, the implants were sectioned in the middle with a water-cooled diamond wire saw (Model 3242, Well, Switzerland) and embedded in epoxy resin. These cross-sections of samples were then sequentially grounded with 40, 20, and 10 µm diamond discs and polished with 7, 3, and 1 µm diamond pastes. A final chemical-mechanical polishing was performed with colloidal silica on a EcoMet250 (Buehler, LakeBluff, IL, US). When zirconia is doped with yttria, the aliovalent substitution of Zr^{4+} with Y^{3+} leads to oxygen vacancies. These vacancies take a leading role in maintaining zirconia in its tetragonal form at room temperature. From the CL point of view, the higher the vacancy concentration, the lower the CL emission intensity (oxygen vacancies would actually disturb energy transfer to the electronic transition responsible for luminescence emission). Nevertheless, LTD is linked to a decrease in oxygen vacancy concentration, by water radicals' adsorption which decreases the stability of metastable tetragonal zirconia and, thus, promotes its transformation into the monoclinic phase. Thus, the monoclinic material recovers luminescence. Therefore, in such material, SEM-CL appears to be a powerful technique to highlight transformed zones by ensuring a field of view unreachable by other characterization modes. Such CL imaging was done using a SEM fitted with a VPSE (Variable Pressure Secondary Electron) detector (SUPRA 55 V P, Carl Zeiss Microscopy GmbH, Oberkochen, Germany). The VPSE detector is a specific arrangement of detectors to obtain SE-similar imaging in the VP mode. Since the VPSE detector detects light, it can be used as a simple CL detector in high vacuum mode. Indeed, it responds to the visible light that is generated by a cathodoluminescent material. Its CL collection efficiency is not optimum, because it is positioned to one side of the specimen, rather than being positioned directly above the specimen, as is the case with purpose-designed collection mirror. Nonetheless thanks to its design, where light is collected and directed into a photomultiplier tube along a transparent glass light guide, the VPSE detector is sufficiently sensitive to low levels of visible light and, as a consequence, is able to function as a panchromatic CL detector. The accelerating voltage for CL imaging was set to 3 keV.

3. Results

3.1. Microstructural features (SEM) of as-received implants

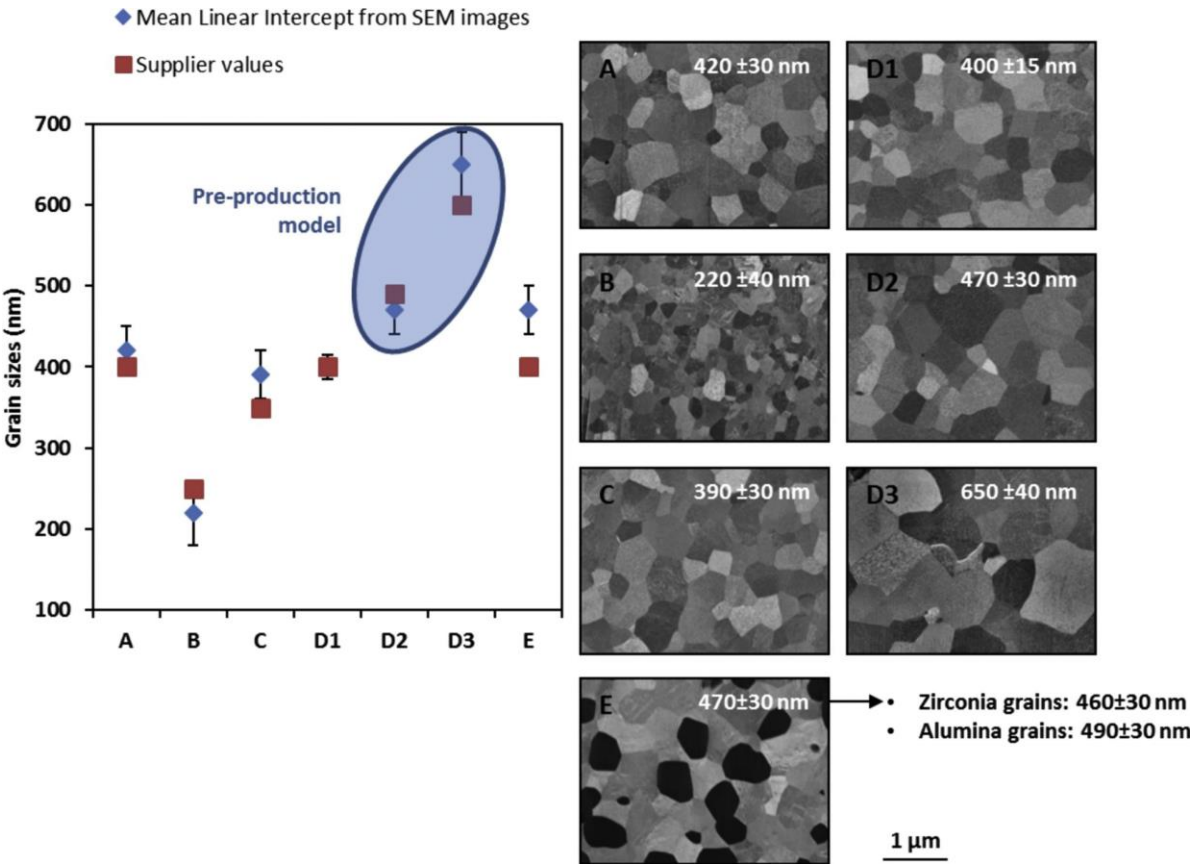

Figure 1: Mean linear intercept measurement chart, SEM presentation and mean grain size measurement for each implant system. A: Z systems® B: Straumann®, C: Zibone®, D1: TAV® dental group 1, D2: TAV® dental group 2, D3: TAV® dental group 3, E: Zeramex®.

For each sample, the grain sizes were measured using the mean linear intercept method (Figure 1). Note that a correction factor of 1.56 was applied to determine the real grain size from the linear intercept segment [26]. Z systems implants exhibited a V-shaped thread design with rounded edges and symmetrical sides inclined at equal angle (Figure 2 a, c). Laser modified roughened surface had a melting structure characterized by symmetrical parallel grooves at the crest of the threads. Straumann implants had a buttress-shaped thread design with sharp square edges and non-symmetrical sides (Figure 3 a, c). Low magnification showed a homogeneous micro-porous structure due to surface etching. Zibone implants presented with V-shaped thread design, rounded edges and symmetrical sides (Figure 4 a, c). Grain accumulations due to annealing and flattened surfaces related to sandblasting were evidenced (Figure 4d-f). TAV dental implants presented with square-threads (Figure 5 a, c). Surface appeared to be sintered following the injection molding. At low magnification, several pores were visible. At high magnification, some areas exhibited a topology of monoclinic grains (uplifts and chevron patterns). Zeramex implants presented square-shaped thread design and a uniform grainy surface similar to Straumann system (Figure 6 a, c). At high magnification etched grains were detected on the surface. Near the polished surface, a combination of grainy and smooth surface as a result of sandblasting could be observed.

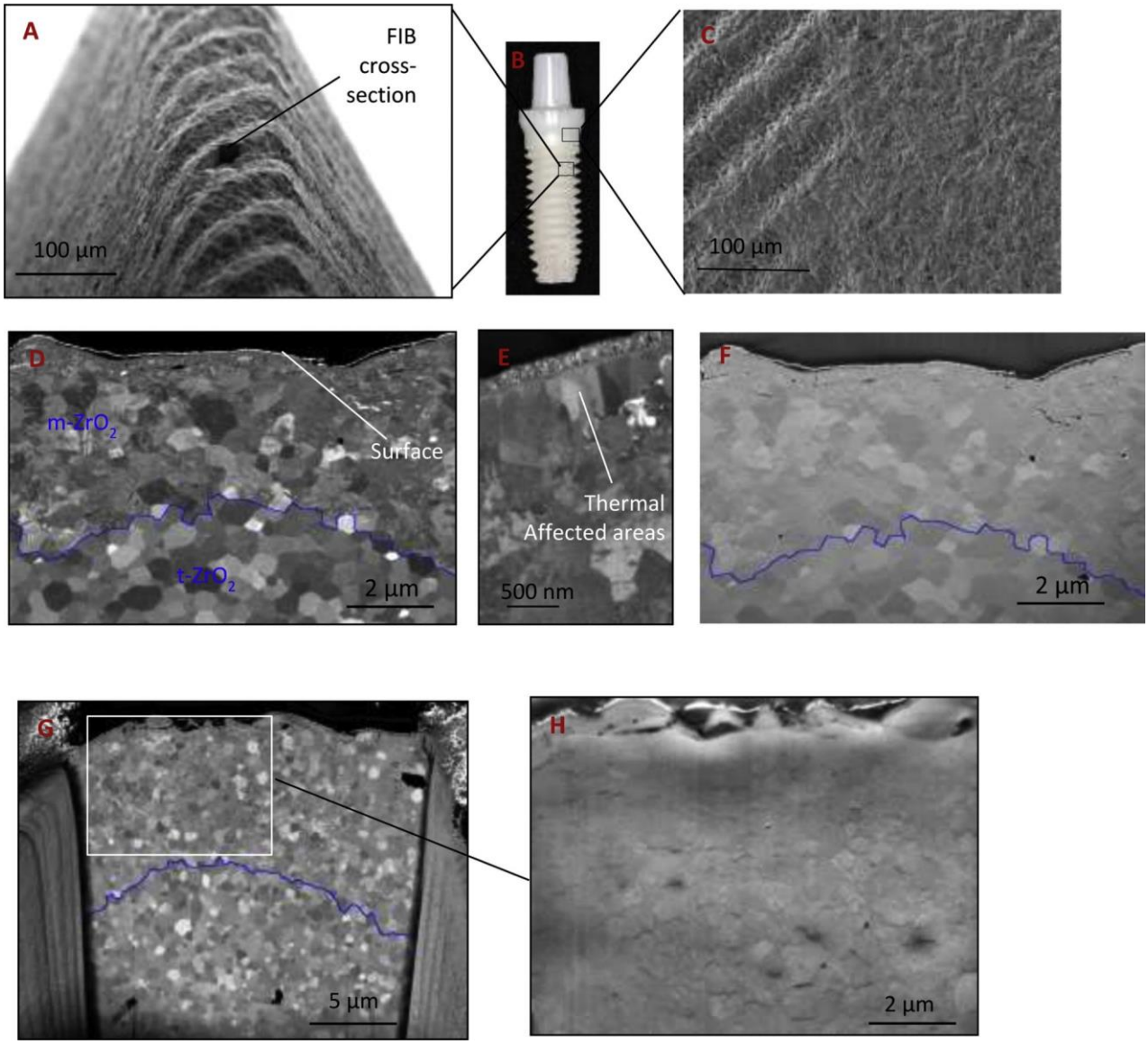

Figure 2: Surface SEM and FIB cross sectional slice of Z systems® before and after ageing. A: Z systems® surface SEM demonstrating the FIB cut over the thread, B: Z systems® implant, C: Surface SEM of implant platform, D-F: FIB cross sectional slice prior to ageing, G-H: FIB cross sectional slice following ageing.

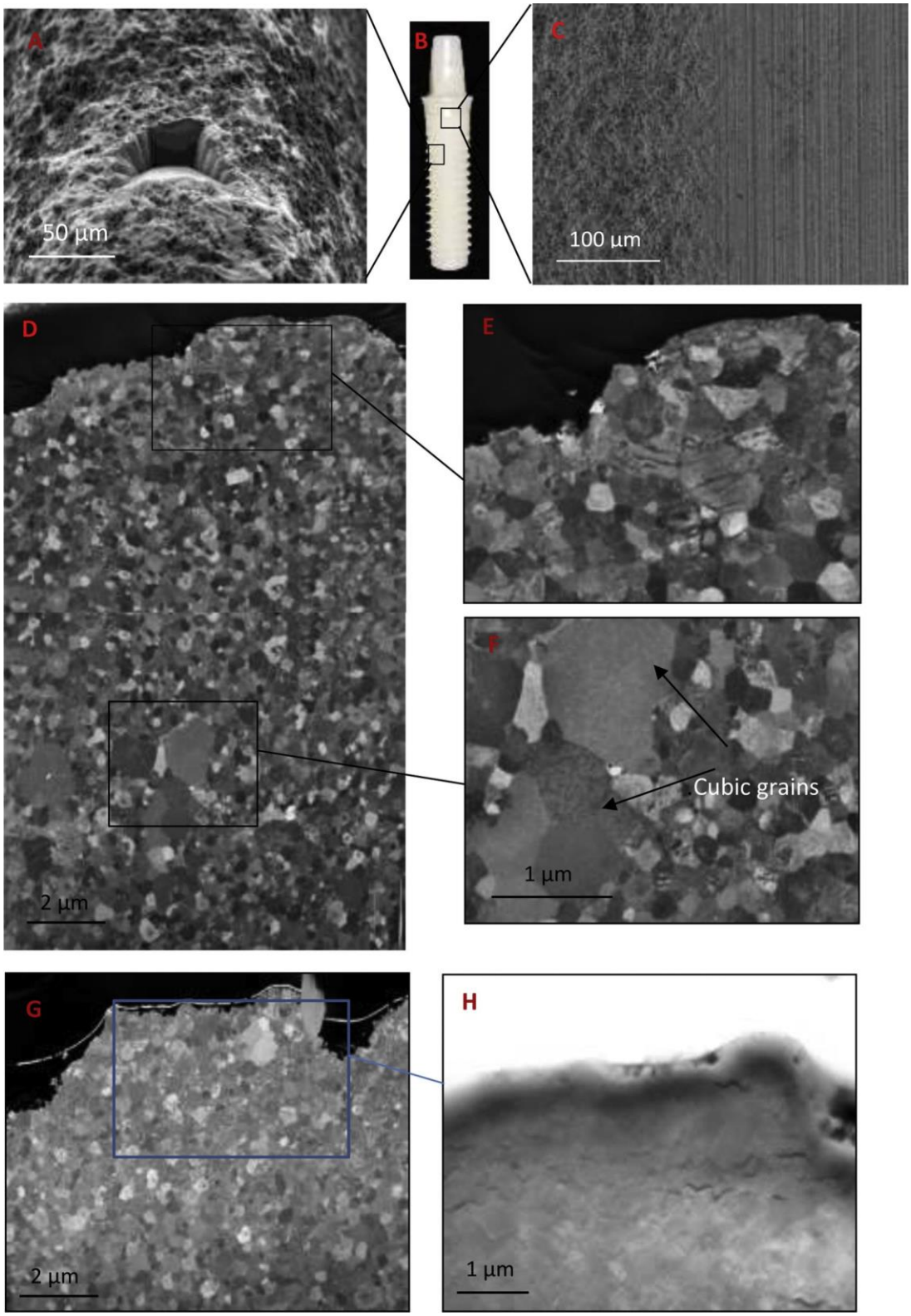

Figure 3: Surface SEM and FIB cross sectional slice of Straumann® before and after ageing. A: Straumann® surface SEM demonstrating the FIB cut over the thread, B: Straumann® implant, C: Surface SEM image of implant platform, D-F: FIB cross sectional cuts prior to ageing, G-H: FIB cross sectional cuts following ageing.

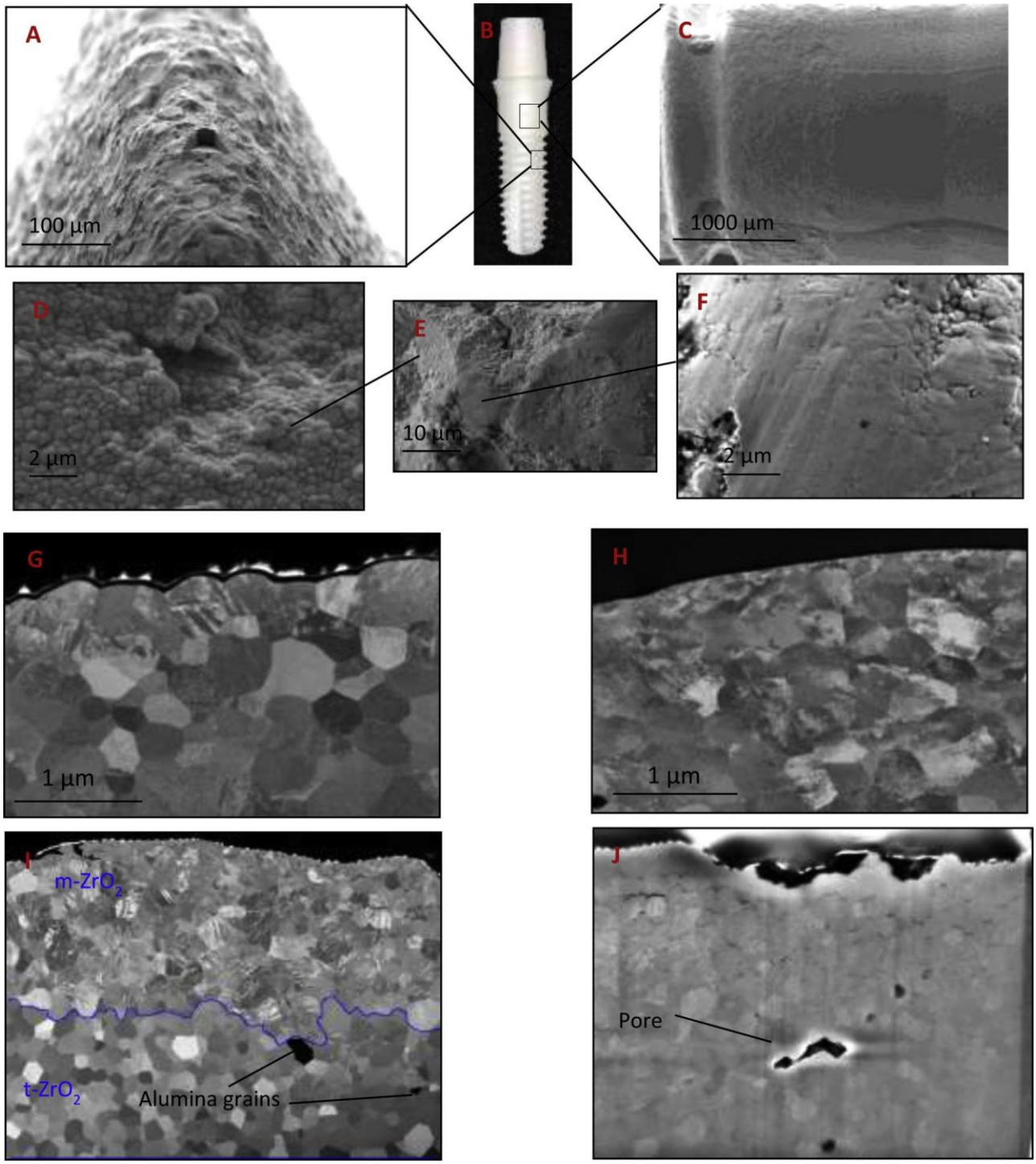

Figure 4: Surface SEM and FIB cross sectional slice of Zibone® before and after ageing. A: Zibone® surface SEM demonstrating the FIB cut over the thread, B: Zibone® implant, C: Surface SEM of implant platform, D: Surface SEM at high magnification demonstrating the grainy area, E: Surface SEM at low magnification demonstrating the grainy and flattened areas, F: Surface SEM at high magnification demonstrating the flattened areas, G-H: FIB cross sectional cut prior to ageing, I-J: FIB cross sectional cuts following ageing.

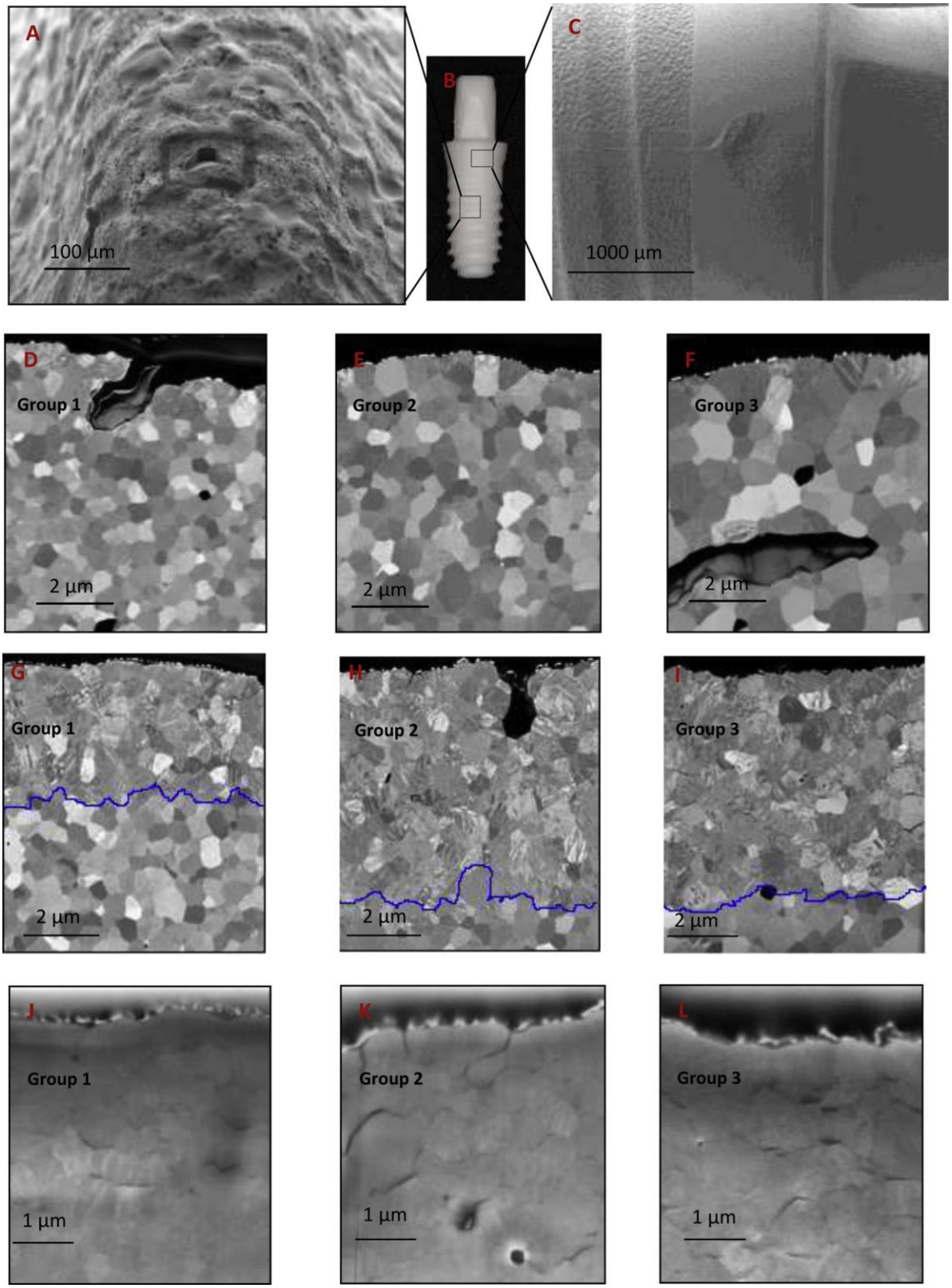

Figure 5: Surface SEM and FIB cross sectional slice of TAV® dental before and after ageing. A: TAV® dental surface SEM demonstrating the FIB cut over the thread, B: TAV® dental implant, C: Surface SEM of implant platform, D-F: FIB cross sectional cuts of group 1 to group 3 prior to ageing, G-I: FIB cross sectional cuts of group 1-3 following ageing, presenting the depth of transformation, J-L: FIB cross section cuts of groups 1-3 following ageing, presenting micro-cracks.

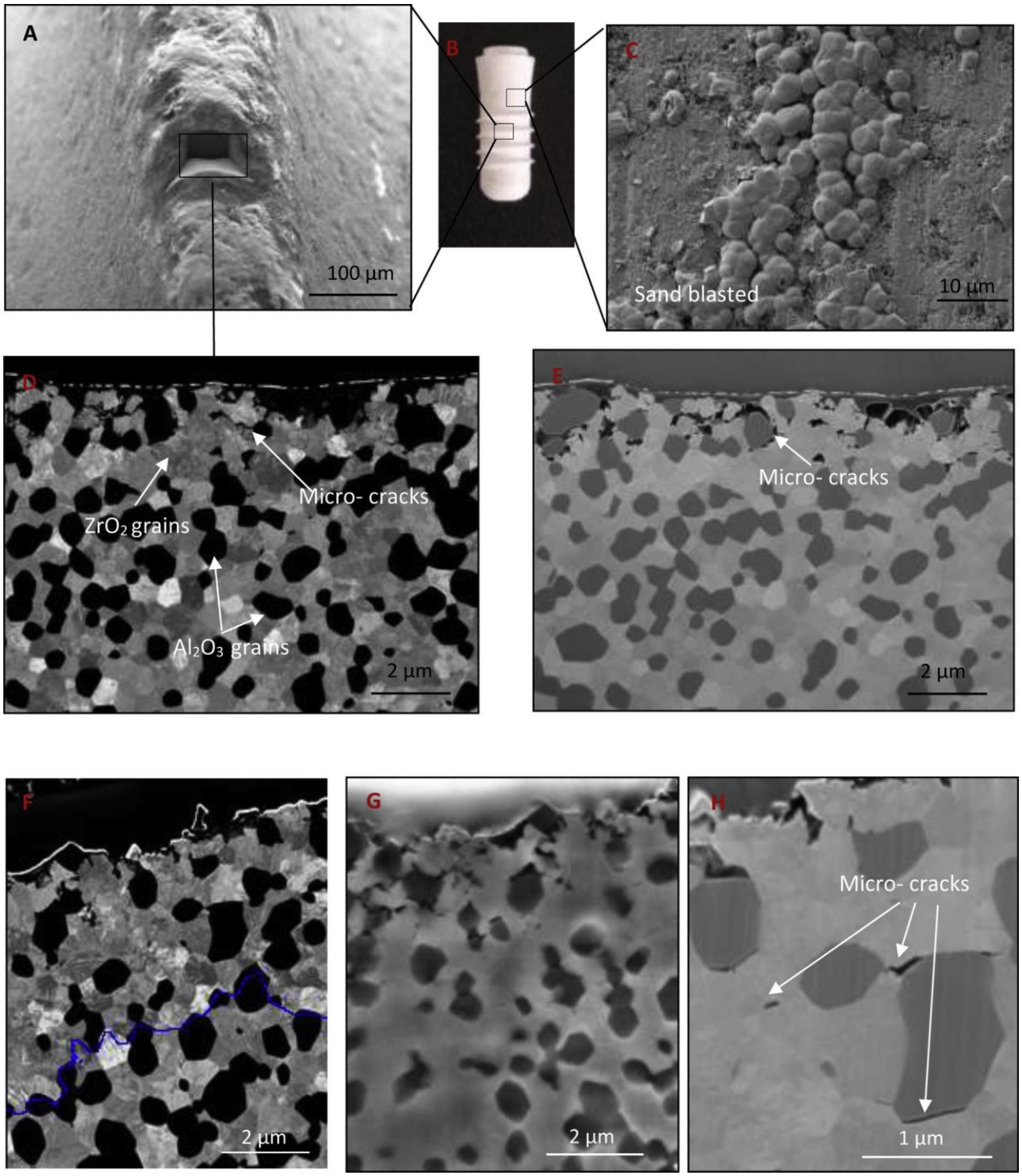

Figure 6: Surface SEM and FIB cross sectional slice of Zeramex® implant before and after ageing. A: Zeramex® surface SEM over the thread presenting the area of cross sectional cut, B: Zeramex® implant, C: Surface SEM of implant platform, D-E: FIB cross sectional cut prior to ageing, F-H: FIB cross sectional cut following ageing.

3.2. SEM of FIB cross sections prior to ageing

Prior to ageing, all implants presented a shallow transformation of grains at the surface (Table 2). Pre-existing micro-cracks were visible in Z systems® and Zeramex® (Table 2). Z systems® presented with columnar grains and micro-cracks of 1.3 ± 1.1 (SD) μm deep (Figure 2 d-f). Evenly distributed alumina grains ≈ 0.5 % were visible in the core structure of Z systems® at polished cross sections (Figure 7). Straumann® had the smallest grain size and presented with some bimodal larger grains that could be cubic grains dispersed uniformly throughout the core structure (Figure 3 f). Zibone® group presented with increase in grain size towards the surface possibly as a result of annealing (Figure 4). TAV dental® implants showed different grain sizes of 0.4 μm, 0.49 μm, and 0.6 μm (Figure 5 d-f). Group 3 (0.6 μm) showed small porosity below the surface with transformed grains along the border of the porosities. Zeramex implant presented with surface porosities and micro-cracks at 1.2 ± 0.3 (SD) μm depth (Figure 6 d, e). Numerous alumina grains along the core were evident in Zeramex implant. Using surface density calculated from a SEM image with a field of view of 32.6 μm x 25 μm after thresholding of more than 600 alumina grains, the content of alumina was estimated to be around 26.6 %.

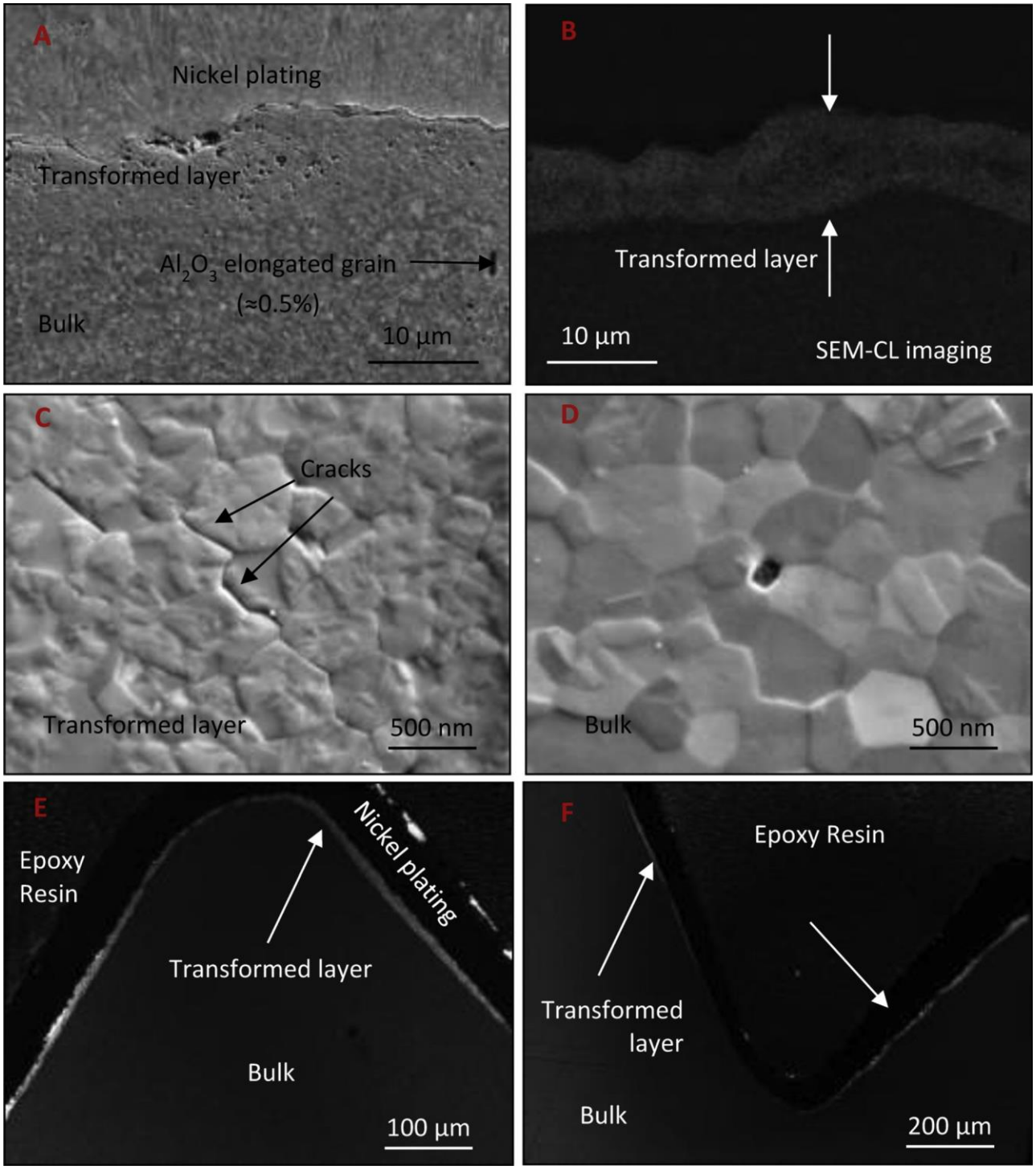

Figure 7: SEM-CL of polished cross sections of Z systems® following ageing duration of 30 h. A: SEM image of Z systems® polished cross section, B: SEM-CL image of Z systems® polished cross section, C: SEM image of transformed layer at high magnification, D: SEM image of non-transformed grains with in the core of the implant at high magnification, E: SEM-CL image at low magnification presenting transformed layer along the thread of the implant, F: SEM-CL image of the transformed layer presented with in the valley of the thread.

Table 2 : Information on monoclinic content, depth of transformation and Micro-crack formation before and after artificial aging (Transformation depths were measured on SEM-CL images for Z systems, Straumann and Zibone aged implants. In this case, about fifty measurements were made for each state on fields of view of 115 µm x 95 µm. In other cases, mean transformation depth was obtained from 15 measures on SEM imaging of one FIB cross-sections.).

	XRD from implant surfaces (0 hr)	Mean transformation depth 0 hr (SD)	Microcrack Depth 0 hr (SD)	XRD from implant surfaces (30 hr)	Mean Transformation depth 30 hr (SD)	Microcrack depth 30 hr (SD)
Z systems® 0.4 µm	39.2 %	4.5 (0.6) µm	1.3 (1.1) µm	56.7 %	7.4 (2.1) µm	6.5 (0.7) µm
Straumann® 0.25 µm	14.4 %	0.3 (0.1) µm	Not visible	74 %	5.1 (1.3) µm	2 (0.4) µm
Zibone® 0.35 µm	14.2 %	0.5 (0.1) µm	Not visible	64.5 %	5.5 (2.6) µm	1.3 (0.4) µm
TAV® group 1 0.4 µm	3.6 %	0.5 (0.1) µm	Not visible	61.2 %	3.4 (0.1) µm	2.6 (0.4) µm
TAV® group 2 0.49 µm	5.1 %	0.4 (0.1) µm	Not visible	73.9 %	6.1 (0.7) µm	4.8 (0.8) µm
TAV® group 3 0.6 µm	9.2 %	0.7 (0.2) µm	Not visible	77.7 %	8.7 (0.4) µm	7.4 (0.5) µm
Zeramex 0.4 µm	58.4 %	2.0 (0.3) µm	1.2 (0.3) µm	77.6 %	4.9 (0.5) µm	2.1 (0.5) µm

3.3. FIB cross-sections of aged implants in BSE and SE mode

All samples showed increase in depth of transformation and micro-crack formation following ageing. Pattern of micro-cracks appeared to be parallel to the surface of the implants. Highest depth of transformation (Table 2) was observed in TAV dental group 3 (0.6 µm) and Z systems followed by TAV dental group 2 (0.49 µm), Zibone, Straumann, Zeramex and TAV dental group 1 (0.4 µm) respectively. The depth of the micro-crack formation from highest to lowest was TAV dental group 3 (0.6 µm), Z systems, TAV dental group 2 (0.49 µm), TAV dental group 1 (0.4 µm), Zeramex, Straumann, and Zibone. Z systems' average depth of t-m transformation and micro-crack formation were 7.4 µm and 6.5 µm respectively. Straumann implants showed an average depth of 5.1 µm t-m transformation and 2 µm of micro-crack formation. Zibone implant presented with 1.3 µm of microcracked zone corresponding to a depth of 5.5 µm transformation. For all TAV dental implants, the zone of transformation and micro-crack formation increased with increasing grain size. TAV dental group 1 (0.4 µm) had the shallowest depth of transformation, corresponding to 3.4 µm and micro-crack zone of 2.6 µm. TAV dental group 2 with intermediate grain size of 0.49 µm showed a transformed zone of 6.1 µm and microcracked depth of 4.8 µm. TAV dental group 3 with the largest grain size (0.6 µm) presented with the highest depth of transformation (8.7 µm) and micro-crack formation (7.4 µm). The micro-cracks were the largest compared to other groups. Lastly, Zeramex implants with alumina stabilized grains showed a transformed zone of 4.9 µm deep and micro- cracks extending to an average of 2.1 µm in the transformed zone. Figure 7, Figure 8, Figure 9 presents cathodoluminescence images of polished cross sections for Z systems, Straumann and Zibone. For Z systems, largest layer of transformation was present on flank of threads followed by the crest of thread and the least amount was seen at root of the thread. It is important to note that laser treatment mainly affected the crest and partially the flanks. For Straumann, the shallowest layer of transformation was present on the crest of the thread with flank and the root having a more uniform layer of transformation. Zibone presented with varying thickness of transformation shown from cathodoluminescence and porosities within the core of the polished cross sections.

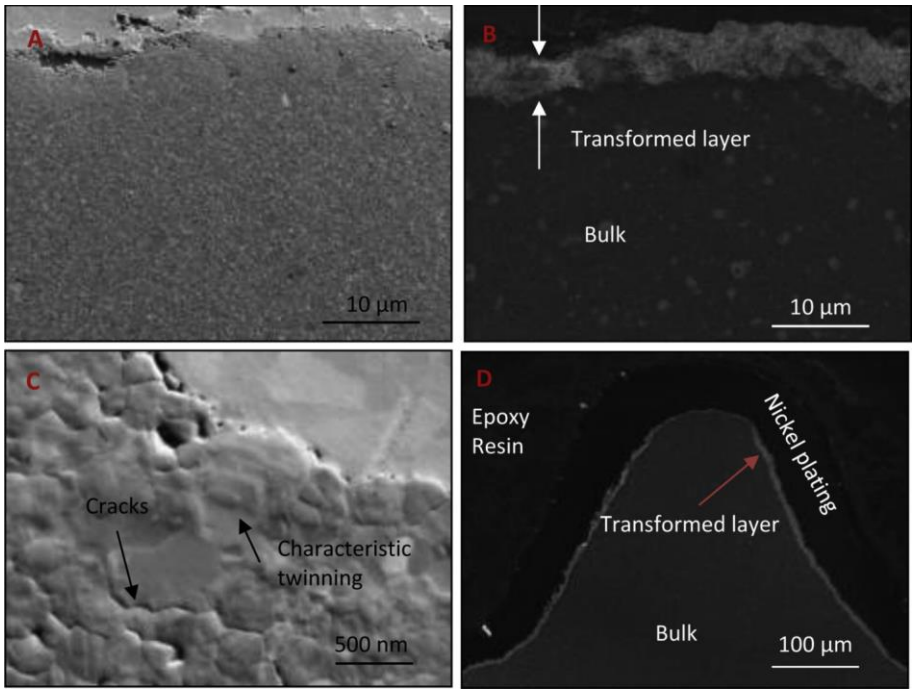

Figure 8 : SEM-CL images of polished cross sections of Straumann® following ageing duration of 30 h. A: SEM image of Straumann® polished cross section, B: SEM-CL image of Straumann® polished cross section, C: SEM image of transformed zone at high magnification, D: SEM-CL image of transformed layer presented over a single thread.

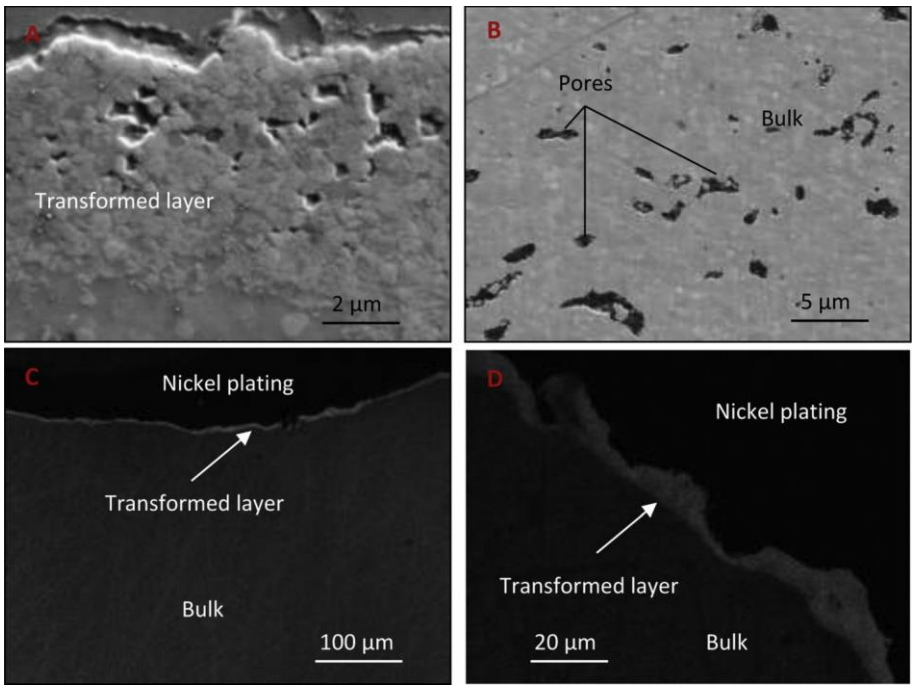

Figure 9: SEM-CL images of polished cross sections of Zibone® following ageing duration of 30 h. A: SEM image of Zibone® polished cross section, B: SEM image of polished cross section with in the core of implant, C: SEM-CL image of polished cross section at low magnification, D: SEM-CL image of polished cross section at high magnification.

3.4. X-Ray diffraction / Degree of phase transformation

The pre-existing monoclinic fractions on the intact surfaces of dental implants are presented in Table 2 from highest to lowest. After the aging process, the monoclinic fractions increased differently, with the highest in TAV group 3 and the lowest in Z-system. The percentage of monoclinic fractions were different than what was measured in FIB cross sectional images in terms of depth and extent of transformation. Figure 10 presents the diffractograms of surface and cross-sectional cuts of aged implants. Different than the XRD results recorded on the implant surfaces showed in Table 2 and Figure 10 b, XRD evaluation on the mechanically sectioned and polished cross sections showed that no monoclinic phase could be detected in the core of any implant. This finding confirms that the polishing procedure used on the cross-section did not induce any t-m phase transformation. Furthermore, the absence of core transformation confirmed that the t-m transformation consecutive to ageing occurs at the surface only.

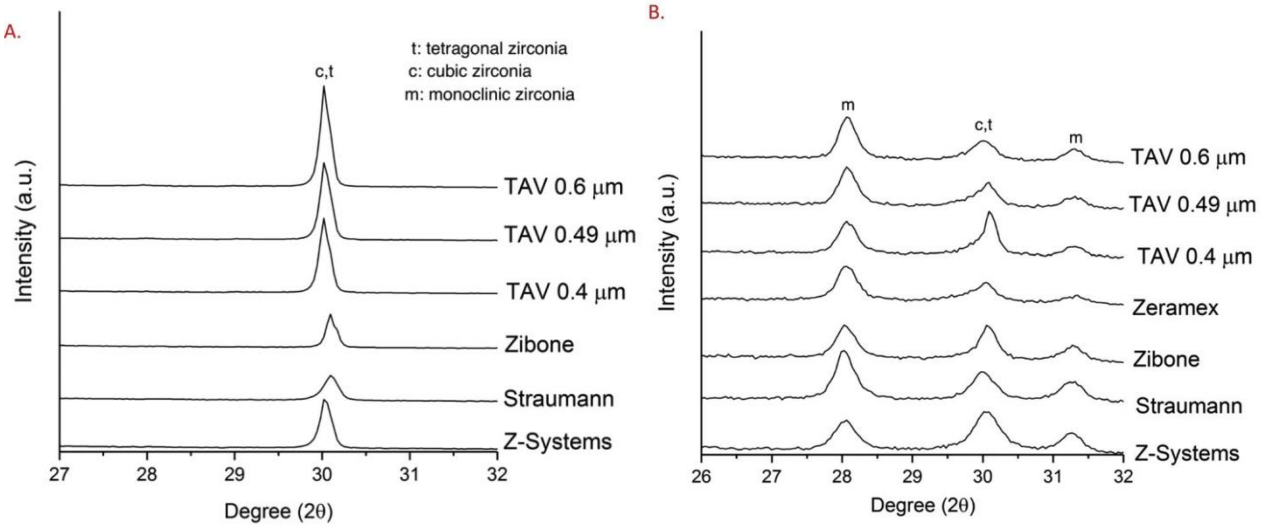

Figure 10: XRD diffractograms of 30 -h aged implants. A: polished cross sections, B: Surface of implants.

4. Discussion

The present study evaluated the microstructural features of 5 commercially and non-commercially available Zirconia dental implants and the effect of LTD *in vitro* on their microstructure. To summarize, the ageing-induced transformation depth was plotted as a function of grain size in Figure 11 a using the data reported in Table 2. Since microcracks were simultaneously detected following the phase transformation (Figure 2, Figure 3, Figure 4, Figure 5, Figure 6) [27], the ratio of increased microcrack depth to increased transformation depth was correlated with grain size in Figure 11 b.

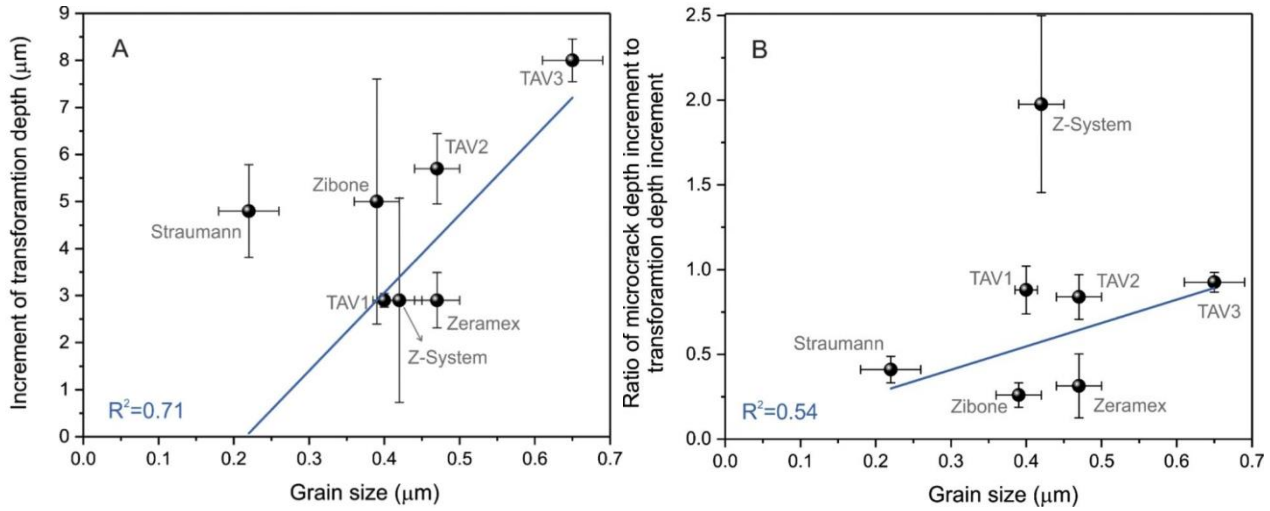

Figure 11: Correlation between grain size and ageing property for all implant systems. TAV1, TAV 2 and TAV3 refer to the group 1, group 2 and group 3 of TAV implants, respectively. Grain sizes were based on the values obtained in this study from SEM images shown in Figure 1. A: Grain size versus the ageing-induced increase of transformation depth. B: Grain size versus microcrack depth increment / transformation depth increment. The solid blue line is the linear regression taking into account of the errors in the X and Y axis and fitting goodness is indicated with R^2. (For interpretation of the references to colour in the Figure, the reader is referred to the web version of this article).

There was a weak correlation between the grain size and the ageing-induced transformation depth with $R^2 = 0.71$ considering all sets of data points (Figure 11 a), suggesting that many other parameters other than the grain size influence the overall ageing-rate of a given zirconia implant. Indeed, as shown in Table 1, all types of implants were processed with quite different technologies, including surface modification. Grain size itself is therefore not enough to predict the sensitivity of a given 3Y-TZP against hydrothermal ageing. On the other hand, TAV samples, which represented the only group with comparable conditions, only different sintering temperature, showed clear evidence of the grain size effect on the depth of the transformed zone as shown through our data points in Figure 11 a. This finding agrees with previous studies on zirconia implants [28] and with extensive work on commercially available and experimentally flat zirconia samples [29,30]. All other process-parameters being the same, a given zirconia ceramic implant is more sensitive to ageing when it exhibits a large grain size. TAV group 3, not available commercially, presented with the least surface treatment, no pre-existing micro-cracks, largest grain size (0.65 ± 0.04 μm) and the least pre-existing transformation, was shown to have the largest transformation and micro-cracked zone after artificial ageing. The depth of transformation increased by ~ 8.0 μm with an average increased micro-crack of 7.4 μm (the entire transformation zone was roughly micro-cracked).

In general as shown in Table 2, the extent of transformation depth is associated to the extent of micro-cracks. However, Figure 11 b shows no correlation between ratio of microcrack depth increment and transformation depth increment to grain size. This finding could be due to small sample size which is a limitation of the present work. It may also depend on microstructural parameters. Ageing of zirconia implant is indeed a complex event influenced by powder preparation, material composition and the

surface treatment, in addition to the influence by grain size. Transformation related micro- cracking may therefore depend on grain size, but also on surface preparation (residual stresses, recrystallization and/or plasticity due to surface modifications) and phase contents (cubic/tetragonal). A more direct analysis can be done on TAV samples, for which the transformed zone is entirely micro-cracked. For these implants, there was no specific surface treatment after sintering. It is believed, thus, that in the case of grains large enough (above a certain threshold value, for which the transformation strains lead to grain-boundary cracking) and when no initial transformed zone is present neither specific residual stresses, that all the transformed zone exhibits a pattern of micro- cracks.

Straumann having the smallest grain size (0.22 ± 0.04 μm) presented with deeper transformation depth than for TAV group 1, Z-system and Zeramex and the value for Straumann implant was clearly deviated from the correlation analysis (blue line in Figure 11 a). Dispersed cubic grains were observed in the microstructure of Straumann implant (Figure 3 d-f), which is different than the other 6 implant systems and could contribute to a deeper transformation depth. The presence of cubic grains was reported to accelerate the ageing-induced transformation rate of Y-TZP ceramics because of the yttrium enrichment in cubic grains and the concomitant depletion of yttrium in the neighboring tetragonal grains [31]. Nevertheless, this did not influence the ageing-induced microcracks in Straumann implant and depth of microcracked zone fell within the correlation analysis with grain size (Figure 11 b). Z-systems on the other hand was strongly susceptible to microcracking. Z-systems presented a particularly high ratio between the increased microcracked zone (~ 5.7 μm) and the increased transformed depth (~ 2.9 μm) - not only the highest ratio amongst all the implant systems but also the only implant that has a ratio > 1, *i.e.* aged-induced microcracked zone was larger than aged-induced transformation zone. This is possibly due to laser treatment of the surface. It has been shown [32,33] that laser patterning of zirconia ceramics alters the surface microstructure due to steep thermal gradient, formation of columnar grains perpendicular to the surface, tetragonal-monoclinic transformation followed by microcrack formation as also observed in our work (Figure 2, Table 2). In addition, the ageing resistance of 3Y-TZP ceramics has been reported to be decreased by laser patterning [33].

Lastly, it is also noteworthy that the shallower transformation zone and less pronounced microcracking in Zeramex in comparison to TAV group 2 (both having grain size of 0.47 ± 0.03 μm) is attributed to the increased volume of alumina grains (25 %) [34].

With regards to our methodology, evidence is provided that unlike FIB, XRD alone is not a reliable technique to evaluate the extent of transformation following ageing [18,28]. After artificial ageing of 30 h, XRD results failed to correspond to FIB findings and did not show significant differences between samples, as most of the information is obtained from the first layers of microns below the surface. Nevertheless, XRD analysis on polished cross sections provided objective data indicating that transformation initiated at the surface as there was no monoclinic phase present within the core of the polished cross sections.

Difference between the results obtained by XRD and FIB can be summarized by the following:

1- FIB is a focused technique (at most 20 × 20 × 20 μm^3), while XRD is performed on several mm^2 at once. Due to the very small volume observed by FIB, FIB data might be less representative than XRD data (obtained on several mm^2). However, one must also consider that XRD data were obtained on very complex surfaces, which may render their analysis difficult. Depending on the sample and the geometry of the surface the average analyzed depth may vary.

2- XRD provides measurements of the monoclinic fractions on the first 5 μm below the surface with the grains closer to the surface having more weight on the result and do not give access to the transformation profile [35]. Although this would be possible in flat samples and with grazing angles [36]. Thereby, the XRD analysis should only be applied to cases with transformation depth < 5 μm.
3- FIB allows the measurement of the transformation depth without giving access to the amount of monoclinic phase in the transformed zone (unless it is coupled to other techniques such as EBSD or state-of-the-art image analysis, which is not the case here).

Cathodoluminescence of polished cross sections of Z-systems and Straumann showed a band of transformation along the crests, flanks and roots of the implants with varying thicknesses. As for both Z systems and Straumann, the transformation was shown to be larger at the flank compared to crest and the root of the threads. It is important to note that varying locations of FIB cross sections may lead to differing results as the thickness of transformed zone can vary along the threads.

Overall, the accelerated ageing resulted in a limited, shallow zone of transformation, with a very small amount of micro- cracking. It was hypothesized that 30 h at 134 °C corresponds to more than 30 years at 37 °C, as was shown for most 3Y-TZP ceramics [10]. This is reached with activation energy for ageing between 90 and 110 kJ/mol [10]. However, recent studies show that the activation energy can vary in large proportions from 40 to 115 kJ/mol in 3Y-TZP ceramics with identical composition but different sintering cycles [37]. Moreover, autoclave conditions by no means can simulate exactly the complex intraoral conditions. Therefore, further *in vivo* studies are necessary to confirm our results. The present observations also provided insights on factors other than grain size including surface treatment, powder preparation, material composition that influence low temperature degradation of dental implants and may be considered in manufacturing processes of commercial implants. In particular, grain size variations *via* changes in sintering temperature is confirmed to be a major factor in the ageing rates. Part II [38] of this project provides additional data about the influence of ageing on mechanical properties of the investigated implants.

Conclusions

- LTD following accelerated ageing of 30 h resulted in
    - Shallow transformation zones in all implant systems.
    - Increased zone of micro-cracks corresponding to the transformation zone.
- Extent of transformation is influenced not only by grain size, which is a primary factor, but also by other parameters such as initial powder and surface treatments.
- Patterns of aged-induced microcracks were parallel to the surface in all groups. The extent of micro-cracking was different from one type of implant to another and did not correlate well with grain size.
- Overall, LTD following *in vitro* ageing using an autoclave for 30 h was minimal for all commercial implant systems investigated, while it represents a quite severe condition.

Declaration of Competing Interest

The authors declare that they have no known competing financial interests or personal relationships that could have appeared to influence the work reported in this paper.

Acknowledgements

This study was supported by Institute National des Sciences Appliquées de Lyon research funds in France. We would like to thank Z-systems, Straumann, TAV Dental, Zibone and Zeramex companies for providing Zirconia dental implants and the CLYM (Centre Lyonnais de Microscopie: www.clym.fr) for providing access to the microscopy facilities and Nicolas Vaché for helping us with the nickel electroplating. The authors have no conflict of interest.

References

1. D.B. Dunn, The use of a zirconia custom implant-supported fixed partial denture prosthesis to treat implant failure in the anterior maxilla: a clinical report, J. Prosth. Dentistry (2008), pp. 415-421
2. R. Glauser, I. Sailer, A. Wohlwend, S. Studer, M. Schibli, P. Scharer, Experimental zirconia abutments for implant supported single tooth restorations in esthetically demanding regions: 4-year results of a propsective clinical study, Int. J. Prosthodontol. (2004), pp. 285-290
3. C. Piconi, G. Maccauro, Zirconia as a ceramic biomaterial, Biomaterials, 1999 (20) (1999), pp. 1-25
4. Scilia, S. Cuesta, G. Coma, I. Arregui, C. Guisasola, E. Ruiz, *et al.*, *T*itanium allergy in dental implant patients: a clinical study on 1500 consecutive patients, Clin. Oral Implants Res., 19 (8) (2008), pp. 823-835
5. R.C. Garvie, R.H. Hannink, R.T. Pascoe, Ceramic Steel?, Nature (1975), pp. 703-704
6. T.K. Gupta, F.F. Lang, J.H. BechtoldEffect of stress-induced phase transformation on the properties of polycrystalline zirconia containing metastable tetragonal phase, J. Mater. Sci. (1977), pp. 1464-1470
7. T.K. Gupta, J.H. Bechtold, R.C. Kuznicki, L.H. Cadoff, B.R. Rossing, Stabilization of tetragonal phase in polycrystalline zirconia, J. Mater. Sci. (1977), pp. 2421-2426
8. K. Kobayashi, H. Kuwajima, T. Masaki, Phase change and mechanical properties of ZrO2-Y2O3 solid electrolyte after ageing, Solid State Ion., 3 (1981), pp. 489-493
9. P.S. Christel, Zirconia: the second generation of ceramics for total hip replacement, Bull. Hosp. Dis. Orthop. Inst., 49 (1988), pp. 170-177
10. J. Chevalier, L. Gremillard, S. Deville, Low-temperature degradation of zirconia and implications for biomedical implants, Annu. Rev. Mater. Res., 37 (2007), pp. 1-32
11. Z. Ozkurt, E. Kazazoglu, Zirconia dental implants: a literature review, J. Oral Implantol., 37 (2011), pp. 367-376
12. M. Andreiotelli, J. Hans, H.J. Wenz, R.J. Kohal, Are ceramic implants a viable alternative to titanium implants? A systematic literature review, Clin. Oral Implants Res., 20 (2009), pp. 32-47
13. P. Kohorst, T.J. Herzog, L. Borchers, M. Stiesch-Scholz, Load- bearing capacity of all-ceramic posterior four-unit fixed partial dentures with different zirconia frameworks, Eur. J. Oral Sci., 115 (2007), pp. 161-166
14. Jerome Chevalier, Laurent Gremillard, Anil V. Virkar, David R. Clarke, The tetragonal-monoclinic transformation in zirconia: lessons learned and future trends, J. Am. Ceram. Soc., 92 (2009), pp. 1901-1920
15. J. Chevalier, J. Loh, L. Gremillard, S. Meille, E. Adolfson, Low-temperature degradation in zirconia with a porous surface, Acta Biomater., 7 (2011), pp. 2986-2993
16. T.F. Alghazzawi, J. Lemons, P.R. Liu, M.E. Essig, A.A. Bartolucci, G.M. Janowski, Influence of low-temperature environmental expo- sure on the mechanical properties and structural stability of dental zirconia, J. Prosthodont., 21 (2012), pp. 363-369
17. P. Kohorst, L. Borchers, J. Strempel, M. Stiesch, T. Hassel, F.W. Bach, C. Hubsch, Low-temperature degradation of different zirconia ceramics for dental applications, Acta Biomater., 8 (2012), pp. 1213-1220
18. C. Sanon, J. Chevalier, T. Douillard, R.J. Kohal, P.G. Coelho, J. Hjerppe, N. Silva, Low temperature degradation and reliability of one-piece ceramic oral implants with a porous surface, Dent. Mater., 29 (2013), pp. 389-397
19. J. Chevalier, J. Loh, L. Gremillard, S. Meille, E. Adolfson, Low-temperature degradation in zirconia with a porous surface, Acta Biomater., 7 (2011), pp. 2986-2993
20. M. Cattani-Lorente, S.S. Scherrer, P. Ammann, M. Jobin, H.W. Wiskott, Low temperature degradation of a Y-TZP dental ceramic, Acta Biomater., 7 (2011), pp. 858-865

21. B.D. Flinn, D.A. Degroot, L.A. Mancl, A.J. Raigrodski, Accelerated aging characteristics of three yttria-stabilized tetragonal zirconia polycrystalline dental materials, J. Prosthet. Dent., 108 (2012), pp. 223-230
22. L. Borchers, M. Stiesch, F.W. Bach, J.C. Buhl, C. Hubsch, T. Kellner, P. Kohorst, M. Jendras, Influence of hydrothermal and mechanical conditions on the strength of zirconia, Acta Biomater., 6 (2010), pp. 4547-4552
23. F.G. Marro, M. Anglada, Strengthening of vickers indented 3Y-TZP by hydrothermal ageing, J. Eur. Ceram. Soc., 32 (2012), pp. 317-324
24. M. Monzavi, S. Noumbissi, H. Nowzari, The impact of in vitro accelerated aging, approximating 30 and 60 years in vivo, on commercially available zirconia dental implants, J. Clin. Implant. Dent. Relat. Res., 19 (2017), pp. 245-252
25. J. Emsley, The Elements (2nd ed.)), Oxford university press, Oxford, Uk (1991)
26. M.I. Mendelson, Average grain size in polycrystalline ceramics, J. Am. Ceram. Soc., 52 (80) (1967), pp. 443-446
27. J.A. Munoz-Tabares, E. Jimenez-Pique, M. Anglada, Subsurface evaluation of hydrothermal degradation of zirconia, Acta Mater., 59 (2011), pp. 473-484
28. C. Sanon, J. Chevalier, T. Douillard, M. Cattani-Lorente, S.S. Scherrer, L. Gremillard, A new testing protocol for zirconia dental implants, Dent. Mater., 31 (2015), pp. 15-25
29. V. Lughi, V. Sergo, Low temperature degradation-aging-of zirconia: a critical review of the relevant aspects in dentistry, Dent. Mater., 26 (2010), pp. 807-820
30. M. Inokoshi, F. Zhang, J. Demunck, S. Minakuchi, I. Naert, J. Vleugels, *et al.*, Influence of sintering conditions on low temperature degradation of dental zirconia, Dent. Mater., 30 (2014), pp. 669-678
31. J. Chevalier, S. Deville, E. Munch, R. Jullian, F. Lair,Critical effect of cubic phase on aging in 3 mol % yttria-stabilized zirconia ceramics for hip replacement prosthesis, Biomaterials, 25 (2004), pp. 5539-5545
32. E. Roitero, F. Lasserre, J.J. Roa, M. Anglada, F. Mucklich, E. Jimenez Pique, Nanosecond-laser patterning of 3Y-TZP: damage and microstructural changes, J. Eur. Ceram. Soc., 37 (2017), pp. 4876-4887
33. E. Roitero, M. Ochoa, M. Anglada, F. Mucklich, E. Jimenez-Pique, Low temperature degradation of laser patterned 3Y-TZP: enhancement of resistance after thermal treatment, J. Eur. Ceram. Soc., 38 (2018), pp. 1742-1749
34. H. Tsubakino, R. Nozaro, M. Hamamoto, Effect of alumina addition on the tetragonal to monoclinic phase transformation zirconia-3 mol% yttria, J. Am. Ceram. Soc., 74 (1991), pp. 440-443
35. F. Zhang, M. Inokoshi, K. Vanmeensel, B. Van Meerbeek, I. Naert, J. Vleugels, Lifetime estimation of zirconia ceramics by linear ageing kinetics, Acta Mater., 92 (2015), pp. 290-298
36. L. Gremillard, S. Grandjean, J. Chevalier, A new method to measure monoclinic depth profile in zirconia-based ceramics from X-ray diffraction data, Int. J. Mater. Res., 101 (2010), pp. 88-94
37. C. Wei, L. Gremillard, Towards the prediction of hydrothermal ageing of 3Y-TZP bioceramics from processing parameters, Acta Materiallia, 144 (2018), pp. 245-256
38. M. Monzavi, F. Zhang, S. Meille, T. Douillard, J. Adrien, S. Noumbissi, H. Nowzari, J. Chevalier, Influence of artificial aging on mechanical properties of commercially and non-commercially available zirconia dental implants, J. Mech. Behav. Biomed. Mater., 101 (2019), p. 103423-103423